

Primal-Dual convex optimization in large deformation diffeomorphic registration with robust regularizers

Monica Hernandez
mhg@unizar.es

Aragon Institute on Engineering
Research (I3A)
University of Zaragoza
Zaragoza, Spain

Abstract

This paper proposes a method for primal-dual convex optimization in variational Large Deformation Diffeomorphic Metric Mapping (LDDMM) problems formulated with robust regularizers and image similarity metrics. The method is based on Chambolle and Pock primal-dual algorithm for solving general convex optimization problems. Diagonal preconditioning is used to ensure the convergence of the algorithm to the global minimum. We study three robust regularizers liable to provide acceptable results in diffeomorphic registration: Huber, V -Huber and Total Generalized Variation. Experiments in a 2D MRI data set with complex geometry show that, for all the considered regularizers, the proposed method is able to converge to diffeomorphic solutions. The method performs similarly to state of the art stationary LDDMM and log-domain diffeomorphic Demons in terms of the image similarity achieved after registration. In addition, evaluation in the 3D Non-Rigid Image Registration Project (NIREP) database shows an acceptable performance for second-order robust regularizers, close to the performance of the state of the art diffeomorphic registration methods.

1 Introduction

Non-rigid image registration is a highly ill-posed problem. This means that a number of qualitatively different transformations can achieve the same image similarity after registration. This justifies the vast literature on image registration methods with differences on transformation characterization, regularizers, image similarity metrics, optimization methods, and additional constraints [27].

In the last decade, diffeomorphic registration has arisen as a powerful paradigm for non-rigid image registration, with application to Computational Anatomy [16, 17, 18]. Large Deformation Diffeomorphic Metric Mapping (LDDMM) [5] and Diffeomorphic Demons [29] are among the most widespread methods for diffeomorphic registration. In both methods, transformations are characterized to belong to an infinite dimensional Riemannian manifold of diffeomorphisms, parameterized by flows of smooth vector fields in the tangent space. The invertibility of the transformations is numerically guaranteed by the use of sufficiently

smooth regularizers [15]. Customarily, these methods regularize the problem with the L^2 -norm of some physically meaningful differential expression of the vector fields [1, 2, 4, 5, 10, 12], or with the Gaussian smoothing of the vector fields [25, 29, 30, 34].

Simultaneously to the development of the diffeomorphic registration paradigm, the computer vision community has shown a growing interest in robust regularizers based on the Total Variation (TV) norm [24]. The popularity of these regularizers has increased thanks to the availability of optimization methods for solving this challenging problem. In particular, Chambolle and Pock proposed a fast first-order primal-dual algorithm for convex optimization and provided the equations for various computer vision problems [7]. Their work recovered the principles of convex analysis and Fenchel-Duality, and derived their primal-dual algorithm from the minimization of a saddle-point problem [22]. This algorithm has been successfully applied to solve different formulations of the optical flow problem [9, 21, 31, 32]. The ability of TV based regularizers to preserve discontinuities has led these methods to occupy top positions in optical flow benchmark studies [3] and non-rigid image registration evaluations [9].

The purpose of this article is to propose a method for primal-dual optimization of convexified LDDMM problems, formulated with robust regularizers and image similarity norms related to the TV norm. The method is based on Chambolle and Pock algorithm with diagonal preconditioning [20]. We study three robust regularizers liable to provide acceptable results in diffeomorphic registration: Huber, V -Huber and Total Generalized Variation (TGV) [6, 33]. The Huber norm is used in the image similarity term. The method is compared in a complex geometry 2D MRI data set with state of the art optical flow and diffeomorphic registration methods. In addition, the 3D version of the method is evaluated with the manual segmentations of the Non Rigid Image Registration Evaluation Project (NIREP) database [26].

In the following, Section 2 describes the variational formulation associated to the convex LDDMM problem, reviews the foundations of primal-dual optimization, and presents the proposed primal-dual LDDMM method. Section 3 shows the experiments performed in 2D and the evaluation in NIREP. Finally, Section 4 gathers the most remarkable conclusions of our work.

2 Method

2.1 Variational formulation

In this section, we adopt the notation used in Beg et al. original V - L^2 variational formulation for the non-stationary LDDMM problem [5]. Let $Diff(\Omega)$ be the manifold of diffeomorphisms. Let V be the corresponding tangent space at the identity. Let $\mathcal{L} = Id - \gamma\Delta$ be the autoadjoint Laplacian operator associated to the scalar product in V , providing the Riemannian metric in $Diff(\Omega)$. The LDDMM variational problem is given by the minimization of the energy functional

$$E(v) = E_{\text{reg}}(v) + \alpha E_{\text{img}}(I_0 \circ \phi_{1,0}^v - I_1), \quad (1)$$

where the regularizer E_{reg} and the image similarity functional E_{img} are typically given by V - and L^2 -norms $E(v) = \langle \mathcal{L}v, \mathcal{L}v \rangle_{L^2} + \alpha \|I_0 \circ \phi_{1,0}^v - I_1\|_{L^2}^2$.

The vector field flow $v \equiv v(t) \in L^2([0, 1], V)$ provides the diffeomorphism parameterization. The transformation $\phi_{1,0}^v$ is the diffeomorphism that warps the source I_0 into the target image

I_1 . It is the solution at time 1 to the transport equation $\frac{d}{dt}\varphi(t) = -v(t) \circ \varphi(t)$ with initial condition $\varphi(0) = id$. This variational formulation is valid for both time-varying and steady velocity field flows, yielding the non-stationary and the stationary LDDMM methods [5, 12].

As a result of the composition of the image with the diffeomorphism $\phi_{1,0}^v$, this energy functional is non-convex. In order to apply Fenchel-Duality principles in the primal-dual optimization of the problem, the functional needs to be transformed into a convex energy [22]. This is approached by computing a first order Taylor expansion of the residual $I_0 \circ \phi_{1,0}^v - I_1$. Thus, $I_0 \circ \phi_{1,0}^v - I_1 \approx I_0 \circ \phi_{1,0}^{v_0} - I_1 + D_v(I_0 \circ \phi_{1,0}^{v_0})(v - v_0)$, where D_v denotes the Frechet differential. The first-order term $D_v(I_0 \circ \phi_{1,0}^{v_0})(v - v_0)$ can be computed from the Gâteaux derivatives associated to v and v_0 , respectively. Thus,

$$D_v(I_0 \circ \phi_{1,0}^v)v = \partial_v(I_0 \circ \phi_{1,0}^v) = (\nabla I_0)^T \circ \phi_{1,0}^v \partial_v \phi_{1,0}^v. \quad (2)$$

The expression of the Gâteaux derivative $\partial_v \phi_{1,0}^v$ depends on the parameterization used for the velocity field v . In this work we use the stationary parameterization and approximate $\partial_v \phi_{1,0}^v$ by $-D\phi_{1,0}^v \cdot v$ using the normal coordinate representation [10, 14].

Gathering these computations, the expression of the convexified variational problem results into

$$E_{conv}(v) = E_{reg}(v) + \alpha E_{img}(I_0 \circ \phi_{1,0}^{v_0} - I_1 + \nabla(I_0 \circ \phi_{1,0}^{v_0})^T v_0 - \nabla(I_0 \circ \phi_{1,0}^{v_0})^T v). \quad (3)$$

In the following, we will denote the convexified expression of E as follows

$$E_{conv}(v) = E_{reg}(v) + \alpha E_{img}(b_{1,0} - A_{1,0}v). \quad (4)$$

2.2 Primal-Dual optimization

Let V, P and Q be three Hilbert vector spaces. Let $K : V \rightarrow P$ and $A : V \rightarrow Q$ be two bounded continuous linear operators. Let $F : P \rightarrow [0, +\infty]$ and $G : V \rightarrow [0, +\infty]$ be two proper, convex and lower-semicontinuous functions involved in the minimization of the primal problem

$$\min_{v \in V} F(Kv) + G(Av). \quad (5)$$

Primal-Dual optimization aims at the minimization of the primal-dual problem

$$\min_{v \in V} \max_{p \in P, q \in Q} \left\langle \begin{pmatrix} K \\ A \end{pmatrix} v, \begin{pmatrix} p \\ q \end{pmatrix} \right\rangle - \begin{pmatrix} F^* \\ G^* \end{pmatrix} \begin{pmatrix} p \\ q \end{pmatrix}, \quad (6)$$

where $F^* : P \rightarrow [0, +\infty]$ and $G^* : Q \rightarrow [0, +\infty]$ are the Legendre-Fenchel transformations or convex conjugates of F and G , respectively. Fenchel-Duality theorem asserts that the primal and the dual problems attain the same solution [22]. Therefore, the minimization of the primal problem (Equation 5) can be approached by finding the saddle point of the primal-dual problem (Equation 6).

Data: $v^0 \in V, \bar{v}_0 \in V, p^0 \in P, q^0 \in Q, \Sigma_p, \Sigma_q, T$ preconditioning matrices, $\theta \in [0, 1]$

Result: $v \in V, p \in P, q \in Q$ solutions of the primal-dual problem

for $n \leftarrow 0$ **to** *maxits* **do**

$$p^{n+1} = (Id + \Sigma_p \partial F^*)^{-1}(p^n + \Sigma_p K \bar{v}^n)$$

$$q^{n+1} = (Id + \Sigma_q \partial G^*)^{-1}(q^n + \Sigma_q A \bar{v}^n)$$

$$v^{n+1} = v^n - TK^* p^{n+1} - TA^* q^{n+1}$$

$$\bar{v}^{n+1} = v^{n+1} + \theta(v^{n+1} - v^n)$$

end

Algorithm 1. Chambolle and Pock algorithm for solving Equation 6.

Chambolle and Pock have recently proposed a first-order primal-dual algorithm for finding the saddle point of the primal-dual problem [7]. It consists in the alternation of a gradient-ascent step in the dual variables, with a gradient-descent step in the primal variables, combined with an extra-gradient step in the primal variable (Algorithm 1). The algorithm can be used whenever the subgradient resolvent operators $(Id + \sigma\partial\cdot)^{-1}$ can be efficiently solved. Since the operator $\mathcal{K} = \begin{pmatrix} K \\ A \end{pmatrix}$ is usually badly scaled, step size selection has been approached using diagonal preconditioning matrices [20]. The diagonal values are computed from the α_p - and $(2 - \alpha_p)$ -norms of the row and column vectors of the matrix expression of operator \mathcal{K} . The parameter $\alpha_p \in [0, 2]$ measures the amount of preconditioning in the primal and the dual spaces, respectively. In this work, we will use $\alpha_p = 1.0$.

This algorithm has been successfully applied to different optical flow and non-rigid sequence registration problems formulated from the minimization of a convex energy in primal-dual form [7, 9, 32].

2.3 Primal-dual LDDMM with robust regularizers

In this work, we consider three different robust regularizers for E_{reg} , and the Huber norm for E_{img} . For each regularizer, we provide the saddle-point problem, Chambolle and Pock primal and dual expressions associated to the minimization of Equation 4, and the operators used for computing the preconditioning matrices. The numerical implementation of the method follows the algorithmic details provided in [31].

2.3.1 Huber regularizer.

The Huber norm is defined as

$$\|x\|_{H_\varepsilon} = \begin{cases} |x| - \varepsilon/2, & \text{if } |x| > \varepsilon \\ |x|^2/(2\varepsilon), & \text{if } |x| \leq \varepsilon \end{cases} \quad (7)$$

where $\varepsilon > 0$ defines the tradeoff between the linear and the quadratic contributions to the norm. The Huber regularizer $\|\nabla v\|_{H_\varepsilon}$ consists in replacing the L^1 norm in the TV regularizer by the Huber norm. Therefore, $\|\nabla v\|_{H_\varepsilon}$ results into an approximation of the TV regularizer with a continuous quadratic expression in the neighborhood at the origin of size 2ε [7].

The convex-conjugate of the Huber norm is given by $(\|\cdot\|_{H_\varepsilon})^*(p) = \frac{\varepsilon\|p\|^2}{2} + \delta_P(p)$, where δ denotes Dirac delta function on the ball of radius one in the dual vector space P [7]. Therefore, the saddle-point problem associated to Equation 4 is given by

$$S(v, p, q) = \langle \nabla v, p \rangle - \frac{\varepsilon\|p\|^2}{2} - \delta_P(p) + \langle b_{1,0} - A_{1,0}v, q \rangle - \frac{\varepsilon\|q\|^2}{2} - \delta_Q(q). \quad (8)$$

The primal and dual equations that iteratively solve this problem using Chambolle and Pock algorithm are

$$\begin{aligned} p^{n+1} &= \Pi_P \left((1 + \varepsilon\Sigma_p)^{-1} (p^n + \Sigma_p \nabla \bar{v}^n) \right) \\ q^{n+1} &= \Pi_Q \left((1 + \varepsilon\Sigma_q)^{-1} (q^n + \alpha\Sigma_q (b_{1,0} - A_{1,0}\bar{v}^n)) \right) \\ v^{n+1} &= v^n - T \cdot \nabla^* p^{n+1} + \alpha T \cdot A_{1,0}^T \cdot q^{n+1}. \end{aligned}$$

The diagonal preconditioning matrices Σ_p , Σ_q and T are built from the matrix associated to the operator $\mathcal{K}_{H_\varepsilon} = \begin{pmatrix} \nabla \\ -\alpha A_{1,0} \end{pmatrix}$.

2.3.2 V -Huber regularizer.

The idea of V -Huber regularizer is to replace ∇ by \mathcal{L} in the definition of Huber regularizer, in order to control the smoothness of the second-order differentials of the vector field. In this case, the saddle-point problem associated to E_{conv} is given by Equation 8, just replacing ∇ by \mathcal{L} . The primal and dual equations that iteratively solve the problem are

$$\begin{aligned} p^{n+1} &= \Pi_P \left((1 + \varepsilon \Sigma_p)^{-1} (p^n + \Sigma_p \mathcal{L} \bar{v}^n) \right) \\ q^{n+1} &= \Pi_Q \left((1 + \varepsilon \Sigma_q)^{-1} (q^n + \alpha \Sigma_q (b_{1,0} - A_{1,0} v^n)) \right) \\ v^{n+1} &= v^n - T \cdot \mathcal{L} p^{n+1} + \alpha \cdot T \cdot A_{1,0}^T \cdot q^{n+1}. \end{aligned}$$

The diagonal preconditioning matrices are built from $\mathcal{K}_{(H_\varepsilon)_V} = \begin{pmatrix} \mathcal{L} \\ -\alpha A_{1,0} \end{pmatrix}$. It should be noticed that the primal-dual version of the convexified original V - L^2 LDDMM problem can be easily obtained from these equations.

2.3.3 Total Generalized Variation (TGV) regularizer.

The TGV-norm is a generalization of the TV-norm that measures the magnitude of high-order differentials [6]. The most popular regularizer is second-order TGV, $TGV_2^{(\alpha_1, \alpha_0)}$, since it provides a good compromise between smoothness and computational complexity. The second-order TGV regularizer is defined as

$$TGV_2^{(\alpha_1, \alpha_0)}(v) = \min_u \alpha_1 \int_{\Omega} |\nabla v - u| d\Omega + \alpha_0 \int_{\Omega} |\nabla u| d\Omega, \quad (9)$$

where ∇u is the symmetric gradient tensor of the matrix field u , $\nabla = (\nabla + \nabla^T)/2$, and the scalars α_1 and α_0 weight the contributions of the first and second-order differentials, respectively.

The saddle-point problem associated to E_{conv} is given by

$$\begin{aligned} S(v, u, p, q, r) &= \langle \nabla v - u, p \rangle - \delta_{P_{\alpha_1}}(p) + \langle \nabla u, q \rangle - \delta_{Q_{\alpha_0}}(q) + \\ &\quad \alpha \langle b_{1,0} - A_{1,0} v, r \rangle - \frac{\varepsilon \|r\|^2}{2} - \delta_R(r), \quad (10) \end{aligned}$$

where $\delta_{P_{\alpha_1}}$ and $\delta_{Q_{\alpha_0}}$ respectively denote Dirac delta function on the balls of radius α_1 and α_0 in the dual spaces P and Q .

Small modifications on Chambolle and Pock primal-dual algorithm, performed to deal with two primal variables and three dual variables [6], yield the primal and dual equations that iteratively solve this problem

$$\begin{aligned} p^{n+1} &= \Pi_{P_{\alpha_1}} (p^n + \Sigma_p (\nabla \bar{v}^n - \bar{u}^n)) \\ q^{n+1} &= \Pi_{Q_{\alpha_0}} (q^n + \Sigma_q \nabla \bar{u}^n) \\ r^{n+1} &= \Pi_R \left((1 + \varepsilon \Sigma_r)^{-1} (r^n + \alpha \Sigma_r (b_{1,0} - A_{1,0} \bar{v}^n)) \right) \\ v^{n+1} &= v^n - T_v \nabla^* p^{n+1} - \alpha T_v A_{1,0}^T r^{n+1} \\ u^{n+1} &= u^n + T_u p^{n+1} - T_u \nabla^* q^{n+1}. \end{aligned}$$

In this case, the diagonal preconditioning matrices are built from $\mathcal{K}_{TGV} = \begin{pmatrix} \nabla & -Id \\ 0 & \nabla \\ -\alpha A_{1,0} & 0 \end{pmatrix}$.

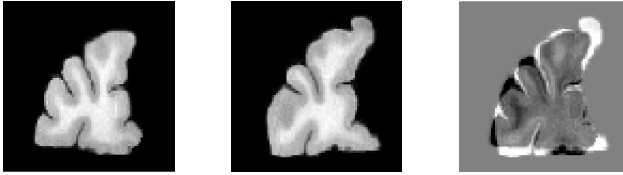


Figure 1: **2D MRI experiment.** Source, target, and residual ($I_0 \circ \phi_{1,0}^v - I_1$) before registration.

3 Results

3.1 Results in 2D MRI

As a proof of concept, we compare primal-dual optimization in $V - L^2$, $H_\varepsilon - H_\varepsilon$, $(H_\varepsilon)_V - H_\varepsilon$, and $TGV - H_\varepsilon$ convex LDDMM problems with primal-dual optimization in $H_\varepsilon - H_\varepsilon$ and $TGV - H_\varepsilon$ convex optical flow problems [32], Gauss-Newton optimization in original $V - L^2$ LDDMM problem [10], and $L^2 - L^2$ log-domain diffeomorphic Demons [28]. The symmetric versions of all the algorithms were used in the comparison. The parameters of the regularizers in the diffeomorphic registration methods were selected in order to provide the minimum image similarity error while keeping the minimum of the Jacobian determinants of the transformations above 0.1 ¹. The parameters of the regularizers in the optical flow methods were selected equal to the parameters of their corresponding diffeomorphic methods.

Experiments were performed in a 2D MRI dataset with complex geometry (Figure 1). Table 1 shows the image similarity error obtained after registration. The error was measured in terms of the L^2 Mean Squared Error of the forward and backward residuals, relative to the first iteration (MSE_r). The table also shows the extrema of the Jacobian determinant associated to the transformations $\phi_{1,0}^v$ and $(\phi_{1,0}^v)^{-1}$ (denoted by $\phi_{0,1}^v$).

All methods were able to achieve acceptable MSE_r values, below 16% in all cases. The lowest errors were obtained by $V - L^2$ LDDMM and diffeomorphic Demons, because both methods include the minimization of the MSE in their optimization. All the diffeomorphic methods provided diffeomorphic solutions for the selected parameters. However, optical flow methods provided non-diffeomorphic solutions. Since these methods do not restrict the transformations to be diffeomorphic, the solutions are allowed to turn into non-diffeomorphic in order to further decrease the image similarity error.

For a qualitative assessment of the registration results, Figure 2 shows the warped sources, residuals, velocity fields, and the obtained transformations for the state of the art and the proposed methods, respectively. From the image of the residuals after registration, it is remarkable the low quality of the registration provided by the optical flow methods, while the proposed primal-dual LDDMM method provides warped sources and residuals visually close to $V - L^2$ LDDMM and diffeomorphic Demons results. The velocity fields and transformations estimated using primal-dual LDDMM show the expected preservation of discontinuities yielded by the robust regularizers and the smoothness of the diffeomorphic characterization.

¹ The smoothness of a given regularizer is related to the parameter selection. For this reason, parameters providing non-diffeomorphic solutions can be found for LDDMM and diffeomorphic Demons [11, 15], and the proposed primal-dual LDDMM method. The choice of parameters providing solutions with minimum Jacobian determinant above the given threshold allows a fair comparison among the methods.

Method	MSE_r ($I_0 \circ \phi_{1,0}^v - I_1$)	MSE_r ($I_1 \circ \phi_{0,1}^v - I_0$)	$\max(J\phi_{1,0}^v)$	$\min(J\phi_{1,0}^v)$	$\max(J\phi_{0,1}^v)$	$\min(J\phi_{0,1}^v)$
$H_\varepsilon - H_\varepsilon$ OF	11.80 %	14.18 %	2.59	-0.53	2.93	0.05
$TGV - H_\varepsilon$ OF	10.95 %	13.38 %	3.39	-1.29	3.55	-0.15
$V - L^2$ GN	8.68 %	9.38 %	2.95	0.14	6.19	0.32
$L^2 - L^2$ DD	10.05 %	12.40 %	7.68	0.16	4.90	0.13
$V - L^2$ PD	11.95 %	11.71 %	4.20	0.10	6.76	0.17
$H_\varepsilon - H_\varepsilon$ PD	14.02 %	13.86 %	2.06	0.29	3.18	0.38
$(H_\varepsilon)_V - H_\varepsilon$ PD	11.90 %	11.68 %	4.45	0.10	6.34	0.16
$TGV - H_\varepsilon$ PD	15.19 %	15.20 %	2.94	0.10	3.11	0.17

Table 1: **2D MRI experiment.** Forward and backward image similarity errors after registration, measured in terms of the MSE relative to the first iteration, and Jacobian determinant extrema associated to the transformations $\phi_{1,0}^v$ and $\phi_{0,1}^v$. OF stands for optical flow, GN for Gauss-Newton, DD for diffeomorphic Demons, and PD for primal-dual.

3.2 Evaluation in 3D NIREP database

Finally, we assess the performance of primal-dual optimization in $V-L^2$, $H_\varepsilon-H_\varepsilon$, $(H_\varepsilon)_V-H_\varepsilon$, and $TGV-H_\varepsilon$ convex LDDMM problems, Gauss-Newton optimization in the original $V-L^2$ problem, and $L^2 - L^2$ log-domain diffeomorphic Demons. The parameters of the regularizers were selected with the same criterion than the 2D MRI data set. Experiments were performed on a NVidia GeForce GTX 760 with 4 GBs of VRAM. The method associated to $TGV-H_\varepsilon$ was implemented in the CPU since its large computational complexity in 3D hindered the execution of experiments in the graphics device.

Table 2 shows the image similarity error and the extrema of the Jacobian determinant obtained after registration, averaged over all the patients. The average of the resulting MSE_r values ranged between 13 and 23%. These values are acceptable for 3D image registration. The lowest errors were obtained by $(H_\varepsilon)_V-H_\varepsilon$ PD method. It is remarkable that the resulting transformations were all diffeomorphic for the selected parameters.

The evaluation is based on the accuracy of the registration results for template-based segmentation of sufficiently locally labeled regions of interest. This evaluation approach has been recommended for obtaining reliable measurements of the performance of non-rigid image registration methods [23]. We use the manual segmentations of the 32 cortical structures provided with the NIREP database as a gold standard. Dice Similarity Coefficient (DSC) is selected as performance metric since this metric (or its related Jaccard coefficient) has been extensively used in the evaluation of registration methods [13, 19, 23]. Thus, given G the gold standard and S the segmentation provided by the registration method, Dice coefficient is defined from the volume of the segmentations as $DSC(G, S) = 2Vol(G \cap S) / (Vol(G) + Vol(S))$.

Method	MSE_r ($I_0 \circ \phi_{1,0}^v - I_1$)	MSE_r ($I_1 \circ \phi_{0,1}^v - I_0$)	$\max(J\phi_{1,0}^v)$	$\min(J\phi_{1,0}^v)$	$\max(J\phi_{0,1}^v)$	$\min(J\phi_{0,1}^v)$
$V - L^2$ GN	16.99 %	16.24 %	6.44	0.23	4.20	0.15
$L^2 - L^2$ DD	14.69 %	15.90 %	5.06	0.13	6.52	0.18
$V - L^2$ PD	18.77 %	20.03 %	7.96	0.17	8.48	0.17
$H_\varepsilon - H_\varepsilon$ PD	21.21 %	22.37 %	3.48	0.16	6.34	0.23
$(H_\varepsilon)_V - H_\varepsilon$ PD	13.21 %	14.10 %	6.69	0.16	9.10	0.12
$TGV - H_\varepsilon$ PD	17.01 %	18.00 %	4.79	0.17	9.34	0.18

Table 2: **3D NIREP experiment.** Mean over the NIREP database of the forward and backward image similarity errors after registration, and Jacobian determinant extrema associated to the transformations $\phi_{1,0}^v$ and $\phi_{0,1}^v$.

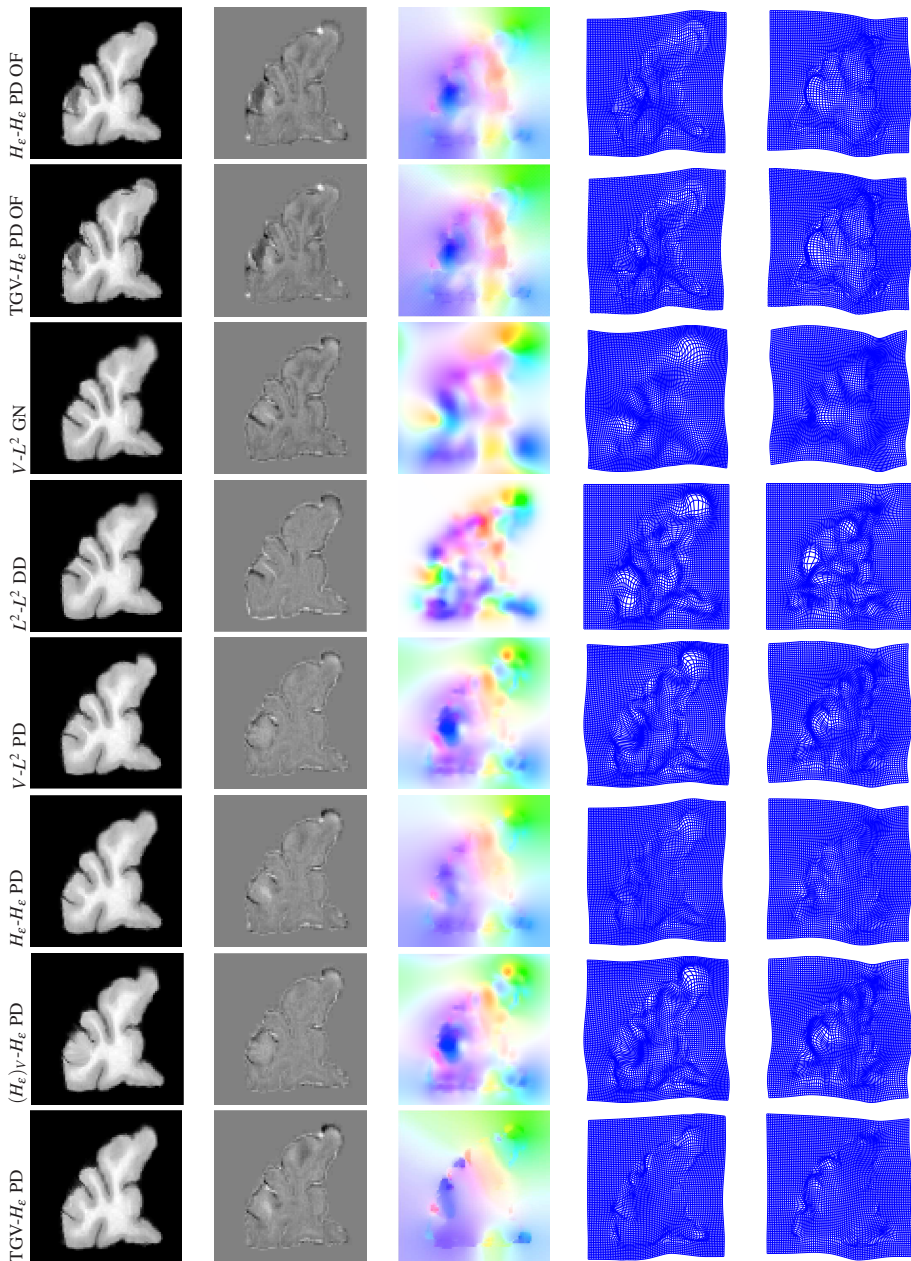


Figure 2: **2D MRI experiment.** Image registration results with the state of the art methods, and the proposed method and the considered regularizers. From left to right, warped sources ($I_0 \circ \phi_{1,0}^v$), residuals ($I_0 \circ \phi_{1,0}^v - I_1$), velocity fields, and grids of $\phi_{1,0}^v$ and $\phi_{0,1}^v$ for the methods considered in the comparison. The velocity fields are colored following Middlebury's coding for optical flow (<http://vision.middlebury.edu/flow>). Grids best viewed with zooming.

Method	mean	std	median	min	max
$V-L^2$ GN	0.5870	0.0852	0.5819	0.3719	0.7197
L^2-L^2 DD	0.6001	0.0887	0.5984	0.3641	0.7394
$V-L^2$ PD	0.5656	0.0869	0.5764	0.3421	0.6873
$H_\epsilon-H_\epsilon$ PD	0.5713	0.0880	0.5673	0.3671	0.7088
$(H_\epsilon)_V-H_\epsilon$ PD	0.6022	0.0843	0.6042	0.3786	0.7311
$TGV-H_\epsilon$ PD	0.5827	0.0849	0.5752	0.3788	0.7189

Table 3: **3D NIREP evaluation.** Overall volume overlap obtained by the registration methods across the 32 regions of interest.

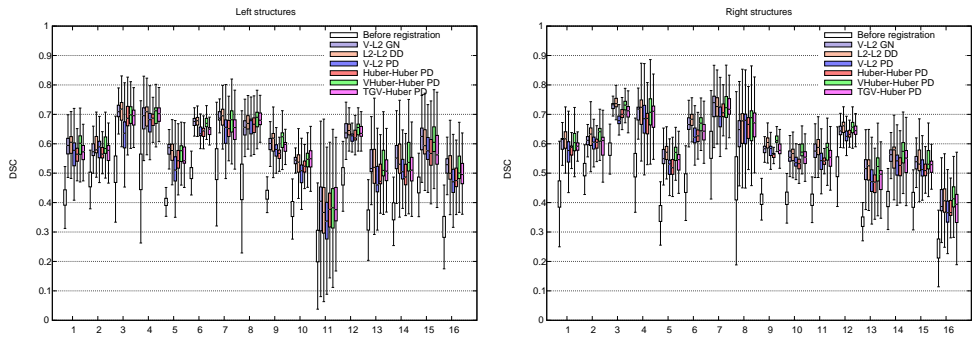


Figure 3: **3D NIREP evaluation.** Volume overlap obtained by the registration methods. Distribution of the Dice coefficients between the deformed and the corresponding manual target segmentations, represented in the shape of box and whisker plots. Best viewed in color and with zooming.

$Vol(S)$). This metric provides the value of 1 if G and S exactly overlap and gradually decreases towards 0 depending on the overlap of the two volumes.

Table 3 shows the most representative statistical measurements of the DSC values obtained by the registration methods computed across the 32 cortical structures. The highest mean and median values with the smallest standard deviation were obtained by $(H_\epsilon)_V-H_\epsilon$ PD method, followed closely by diffeomorphic Demons. $V-L^2$ Gauss-Newton LDDMM and $TGV-H_\epsilon$ PD performed similarly. The lowest mean and median values were obtained by $H_\epsilon-H_\epsilon$ and $V-L^2$ PD methods.

Figure 3 shows the statistical distribution of the DSC values obtained before and after registration for each cortical structure. The second-order optimization methods (i.e. $V-L^2$ Gauss-Newton LDDMM and diffeomorphic Demons) performed similarly in the great majority of cases. These methods usually outperformed $V-L^2$ PD method. From the robust regularizers, $H_\epsilon-H_\epsilon$ regularizer tended to perform similarly to $V-L^2$ primal-dual method, usually with the worst scoring methods. It is remarkable the performance of $(H_\epsilon)_V-H_\epsilon$, usually with the best scoring methods for each region. The performance of the $TGV-H_\epsilon$ regularizer was usually in between the best and the worst scoring methods.

Finally, Table 4 shows the computational complexity of the methods at the highest resolution level. Although PD methods had greater memory requirements than diffeomorphic Demons, they outperformed both diffeomorphic Demons and $V-L^2$ Gauss-Newton LDDMM in terms of the computational time. The most efficient method was $H_\epsilon-H_\epsilon$ PD, followed by $V-L^2$ and $(H_\epsilon)_V-H_\epsilon$ PD methods.

Method	$V - L^2$ GN	$L^2 - L^2$ DD	$V - L^2$ PD	$H_\varepsilon - H_\varepsilon$ PD	$(H_\varepsilon)_V - H_\varepsilon$ PD	$TGV - H_\varepsilon$ PD
VRAM peak memory (MBs)	4046	3272	4047	3840	4047	27000 _(CPU)
Time (seconds)	281.46	234.24	195.89	104.43	206.59	3248.83 _(CPU)

Table 4: **3D NIREP evaluation.** Computational complexity at the highest resolution level (image dimension $180 \times 210 \times 180$). For comparison purposes, the time for $V - L^2$ GN and DD is provided after 100 iterations. The time for PD methods is provided after 5 warps with 20 iterations per warp.

4 Conclusions

In this work, we have proposed a method for primal-dual optimization in convex LDDMM variational problems with robust regularizers and image similarity metrics. To our knowledge, this is the first attempt to include robust regularizers in diffeomorphic registration.

Results in the 2D MRI data set have demonstrated that diffeomorphic solutions can be obtained for Huber, V-Huber and TGV regularizers, despite the preservation of discontinuities favored by the robust regularizers. The method has shown to be able to perform similarly to state of the art diffeomorphic registration methods in terms of the image similarity after registration.

The evaluation in the NIREP database has shown a comparable performance for V-Huber regularizer with respect to the original $V - L^2$ variational formulation and $L^2 - L^2$ log-domain diffeomorphic Demons. For each region, the results obtained by V-Huber regularizer were with the best scoring methods. $V - L^2$ and Huber regularizers consistently underperformed in some regions. The performance of TGV regularizer was usually located above the worst performing methods and slightly below the best performing methods. In some cases, TGV regularizer was with the best scoring methods. Moreover, primal-dual optimization methods (except TGV) were more efficient than diffeomorphic Demons, widely used because of its computational efficiency.

Although the most direct area of application of the proposed method is medical imaging in Computational Anatomy, we believe that diffeomorphic registration with robust regularizers may be applied to estimate diffeomorphic optical flow in non-rigid scenes of the real world. Diffeomorphic solutions may improve the performance of methods for non-rigid structure from motion and 3D non-rigid scene understanding that use optical flow correspondences as input [8]. This will be our objective in future work.

Acknowledgements

The author would like to acknowledge the anonymous reviewers for their revision of the manuscript. This work was partially supported by MINECO Spanish projects DPI2012-32168 and DPI2012-31781.

References

- [1] J. Ashburner. A fast diffeomorphic image registration algorithm. *Neuroimage*, 38(1): 95 – 113, 2007.

- [2] J. Ashburner and K. J. Friston. Diffeomorphic registration using geodesic shooting and gauss-newton optimisation. *Neuroimage*, 55(3):954 – 67, 2011.
- [3] S. Baker, D. Scharsteing, J.P. Lewis, S. Roth, M. J. Black, and R. Szeliski. A database and evaluation method for optical flow. *Int. J. Comput. Vision*, 92:1 – 31, 2011.
- [4] M. F. Beg and A. Khan. Symmetric data attachment terms for large deformation image registration. *IEEE Trans. Med. Imaging*, 26(9):1179 – 1189, 2007.
- [5] M. F. Beg, M. I. Miller, A. Trouve, and L. Younes. Computing large deformation metric mappings via geodesic flows of diffeomorphisms. *Int. J. Comput. Vision*, 61 (2): 139–157, 2005.
- [6] K. Bredies, K. Kunisch, and T. Pock. Total generalized variation. *SIAM J. Imaging Sciences*, 3(3):492 – 526, 2009.
- [7] A. Chambolle and T. Pock. A first-order primal-dual algorithm for convex problems with applications to imaging. *J. Math. Imaging Vis.*, 40(1):120 – 145, 2011.
- [8] R. Garg, A. Roussos, and L. Agapito. Dense variational reconstruction of non-rigid surfaces from monocular video. *Proc. of the IEEE Computer Society Conference on Computer Vision and Pattern Recognition (CVPR'13)*, 2013.
- [9] R. Garg, A. Roussos, and L. Agapito. A variational approach to video registration with subspace constraints. *Int. J. Comput. Vision*, 104(3):286 – 314, 2013.
- [10] M. Hernandez. Gauss-Newton inspired preconditioned optimization in large deformation diffeomorphic metric mapping. *Phys. in Med. and Biol.*, 59(20), 2014.
- [11] M. Hernandez, X. Pennec, and S. Olmos. Comparing algorithms for diffeomorphic registration: stationary LDDMM and diffeomorphic Demons. *Proc. of the 2st International Workshop on Mathematical Foundations of Computational Anatomy (MFCA'08)*, 2008.
- [12] M. Hernandez, M. N. Bossa, and S. Olmos. Registration of anatomical images using paths of diffeomorphisms parameterized with stationary vector field flows. *Int. J. Comput. Vision*, 85 (3):291 – 306, 2009.
- [13] A. Klein, J. Andersson, B. A. Ardekani, J. Ashburner, B. Avants, M. C. Chiang, G. E. Christensen, D. L. Collins, J. Gee, P. Hellier, J. H. Song, M. Jenkinson, C. Lepage, D. Rueckert, P. Thompson, T. Vercauteren, R. P. Woods, J. J. Mann, and R. V. Parsey. Evaluation of 14 nonlinear deformation algorithms applied to human brain MRI registration. *Neuroimage*, 46(3):786–802, 2009.
- [14] R. Mahony and J. H. Manton. The geometry of the Newton method on non-compact Lie groups. *Journal of Global Optimization*, 23:309 – 327, 2002.
- [15] A. Mang and G. Biros. An inexact Newton-Krylov algorithm for constrained diffeomorphic image registration. *SIAM Journal on Imaging Sciences*, 2015.
- [16] M. I. Miller. Computational anatomy: shape, growth, and atrophy comparison via diffeomorphisms. *Neuroimage*, 23:19–33, 2004.

- [17] M. I. Miller and A. Qiu. The emerging discipline of computational functional anatomy. *Neuroimage*, 45(1):16–39, 2009.
- [18] M. I. Miller, A. Banerjee, G. Christensen, S. Joshi, N. Khaneja, U. Grenander, and L. Matejic. Statistical methods in Computational Anatomy. *Stat. Methods Med. Res.*, 6:267 – 299, 1997.
- [19] Y. Ou, H. Akbari, M. Bilello, X. Da, and C. Davatzikos. Comparative evaluation of registration algorithms in different brain databases with varying difficulty: results and insights. *IEEE Trans. Med. Imaging*, 33(10):2039 – 2065, 2014.
- [20] T. Pock and A. Chambolle. Diagonal preconditioning for first order primal-dual algorithms in convex optimization. *Proc. of the 13th IEEE International Conference on Computer Vision (ICCV’11)*, 2011.
- [21] R. Ranftl, K. Bredies, and T. Pock. Non-local total generalized variation for optical flow estimation. *Proc. of the 13th European Conference on Computer Vision (ECCV’14), Lecture Notes in Computer Science (LNCS), Springer- Verlag, Berlin, Germany*, 8689: 439 – 454, 2014.
- [22] R.T. Rockafellar. Convex analysis. *Princeton Landmarks in Mathematics. Princeton University Press, Princeton*, 1977.
- [23] T. Rohlfing. Image similarity and tissue overlaps as surrogates for image registration accuracy: widely used but unreliable. *IEEE Trans. Med. Imaging*, 31(2):153 – 163, 2012.
- [24] L. Rudin, S. Osher, and E. Fatemi. Nonlinear total variation based noise removal algorithms. *Physica D*, 60:259 – 268, 1992.
- [25] S. Sommer, F. Lauze, M. Nielsen, and X. Pennec. Sparse multi-scale diffeomorphic registration: the kernel bundle framework. *J. Math. Imaging Vis.*, 46(3):292 – 308, 2013.
- [26] J. H. Song, G. E. Christensen, J. A. Hawley, Y. Wei, and J. G. Kuhl. Evaluating image registration using NIREP. *Proc. of 7th International Workshop on Biomedical Image Registration (WBIR’10)*, 6204:140 – 150, 2010.
- [27] A. Sotiras, C. Davatzikos, and N. Paragios. Deformable medical image registration: A survey. *IEEE Trans. Med. Imaging*, 32(7):1153 – 1190, 2013.
- [28] T. Vercauteren, X. Pennec, A. Perchant, and N. Ayache. Symmetric log-domain diffeomorphic registration: A demons-based approach. *Proc. of the 11th International Conference on Medical Image Computing and Computer Assisted Intervention (MICCAI’08), Lecture Notes in Computer Science (LNCS), Springer- Verlag, Berlin, Germany*, pages 754 – 761, 2008.
- [29] T. Vercauteren, X. Pennec, A. Perchant, and N. Ayache. Diffeomorphic demons: Efficient non-parametric image registration. *Neuroimage*, 45(1):S61 – S72, 2009.
- [30] F. X. Vialard, L. Risser, D. Rueckert, and C. J. Cotter. Diffeomorphic 3D image registration via geodesic shooting using an efficient adjoint calculation. *Int. J. Comput. Vision*, 97(2):229 – 241, 2012.

- [31] A. Wedel, T. Pock, C. Zach, H. Bischof, and D. Cremers. An improved algorithm for TV-L1 optical flow. *SGAVMA 2009, Lecture Notes in Computer Science*, 5640:23 – 45, 2009.
- [32] M. Werlberger. Convex approaches for high performance video processing. *Ph.D. thesis*, 2012.
- [33] M. Werlberger, W. Trobin, T. Pock, A. Wedel, D. Cremers, and H. Bischof. Anisotropic Huber-L1 optical flow. *Proc. of British Machine Vision Conference (BMVC'09)*, 2009.
- [34] L. Younes. Jacobi fields in groups of diffeomorphisms and applications. *Q. Appl. Math.*, 65:113 – 134, 2007.